Acta Cryst. (1987). A43, 212-216

Determination of Precise X-ray Diffraction Angles by Fast Fourier Transform

BY S. TOKITA AND T. KOJIMA

Department of Electrical Engineering, Salesian Polytechnic, 2-35-11, *Igusa, Suginami-ku, Tokyo* 167, *Japan*

AND I. NISHIDA

National Research Institute for Metals, 2-3-12, *Nakameguro, Meguro-ku, Tokyo* 153, *Japan*

(*Received* 14 *February* 1986; *accepted* 9 *September* 1986)

Abstract

A new analytical method is presented for the separation of two or more closely overlapping X-ray diffraction lines using the narrowly distributed Gaussian function and one-dimensional fast Fourier transform pair. To test the method, the diffraction lines associated with characteristic $K\alpha_1$ and $K\alpha_2$ rays are measured by an X-ray diffractometer using a Brazilian quartz powder as a standard sample. It is found that the observed diffraction lines can be completely separated into $K\alpha_1$ and $K\alpha_2$ lines and that the accuracy of those diffraction angles is better than 2×10^{-4}.

1. Introduction

The accuracy of a lattice constant in material as measured by an X-ray diffractometer depends entirely upon the observed diffraction angles. Although systematic and accidental errors are unavoidable, statistical errors can be reduced by using more data. In the determination of precise lattice constants, therefore, a large number of data must be observed correctly by some X-ray diffraction technique. However, it is unavoidable that the diffraction distribution of characteristic X-rays $K\alpha_1$ and $K\alpha_2$ for small diffraction angles overlaps greatly. This often makes it impossible to decide the exact diffraction angles by adopting ordinary peak-search methods. The common procedure for determining the diffraction angles is to construct diagrams of diffraction lines and to obtain their medium point of angular width at half-maximum intensity from the observed intensities. This procedure is not feasible in the case of closely overlapping diffraction lines.

For well resolved peaks, diffraction angles can be determined as the angles where the first derivative of the line profile is zero or as the mean of angular values on the wings of the profile where the second derivative is zero. This method is used in the Philips PW1700 powder diffractometer system (Philips, 1983) and is capable of rapid analysis, giving satisfactory data for identification purposes. However, when two or more diffraction lines overlap, the diffraction angles calculated become increasingly ambiguous if not indeterminable.

The purpose of the present work is to separate overlapping lines associated with the $K\alpha_1$ and $K\alpha_2$ distribution and thus determine the precise diffraction angles by adopting the one-dimensional fast Fourier transform pair (Cooley & Tukey, 1965) and narrowly distributed Gaussian function to an X-ray diffraction pattern.

2. Separation of overlapping diffraction patterns

The diffracted intensity distribution is composed of contributions from the characteristic $K\alpha_1$ and $K\alpha_2$ X-rays. The diffraction spectra of $K\alpha_1$ and $K\alpha_2$ can be described by the impulse symbol $\delta(\varphi)$ (Bracewell, 1978) as

$$I_1\delta[\varphi-\varphi_1(hkl)], \qquad (1a)$$

$$I_2\delta[\varphi-\varphi_2(hkl)], \qquad (1b)$$

where φ corresponds to the observed angle 2θ; φ_1 and φ_2 are the theoretical diffraction angles $2\theta_1$ from the $K\alpha_1$ and $2\theta_2$ from the $K\alpha_2$ component, respectively. I_1 and I_2 are the diffracted intensities contributed by $K\alpha_1$ and $K\alpha_2$, respectively. A typical intensity distribution is shown in Fig. 1. The shape is due to the crystalline microstrain, to the uneven X-ray diffraction caused by atomic thermal vibration within unit cells, and also to the finite width of the incident X-ray beam. This intensity distribution can be separated into two single distribution functions $W(\varphi)$ (dotted curves in Fig. 1). The function $X(\varphi)$ for the measured intensity distribution (solid curve) in the narrow range $\varphi_0\le\varphi\le\varphi_n$ on the φ axis is expressed as

$$X(\varphi)=[I_1/W(0)]W[\varphi-\varphi_1(hkl)]+[I_2/W(0)]W[\varphi-\varphi_2(hkl)], \qquad (2)$$

where $W(0)$ is the value of $W(\varphi)$ when $\varphi=0$.

The diffraction angle for either characteristic $K\alpha_1$ or $K\alpha_2$ rays and the distribution function $W(\varphi)$ must be previously known to separate the two distribution curves on the φ axis using (2). As a means of finding the diffraction angle, we put $\varphi_0=0$ at an arbitrary point along the extended line of the φ axis and define a new symmetrical function, which in the interval

0108-7673/87/020212-05$01.50

$-\varphi_n \le \varphi \le \varphi_n$ is expressed as

$$X(\varphi) = [I_1/W(0)]\{W[\varphi - \varphi_1(hkl)] + W[\varphi + \varphi_1(hkl)]\} + [I_2/W(0)]\{W[\varphi - \varphi_2(hkl)] + W[\varphi + \varphi_2(hkl)]\}. \quad (3)$$

The pattern given by (3) can be regarded as the one-dimensional Fourier transform pattern of the product of the wave $x(\nu)$ which combines two cosine waves with different frequencies on the $1/\varphi$ axis (call it the ν axis), and the distribution function $w(\nu)$ which peaks at $\nu = 0$, *i.e.*

$$X(\varphi) = \int_{-\infty}^{\infty} x(\nu) w(\nu) \exp(-2\pi i \nu \varphi)\, d\nu, \quad (4)$$

where $x(\nu)$ contains information about the locations of the diffraction lines from the $K\alpha_1$ and $K\alpha_2$ radiation. The exact diffraction angles may be obtained if $x(\nu)$ can be calculated from $X(\varphi)$. $X(\varphi)$ is expressed as the convolution of the distribution function $W(\varphi)$ and the diffraction spectra of $K\alpha_1$ and $K\alpha_2$, and is a positive real function. Hence the inverse Fourier transform is applied to (3) in the range $-\varphi_n \le \varphi \le \varphi_n$, and then

$$\int_{-\varphi_n}^{\varphi_n} X(\varphi) \exp(2\pi i \nu \varphi)\, d\varphi = x(\nu) w(\nu) = \{[2I_1/W(0)] \cos 2\pi\nu\varphi_1'(hkl) + [2I_2/W(0)] \cos 2\pi\nu\varphi_2'(hkl)\} w(\nu) \quad (5)$$

(Betts, 1970), where $\varphi_1' = \varphi_1 - \varphi_0$, $\varphi_2' = \varphi_2 - \varphi_0$. By numerical analysis of (5), $w(\nu)$ is determined from the envelope of $x(\nu)w(\nu)$ and then the composite wave $x(\nu)$ can be obtained. $x(\nu)$ is composed of the sum of the two waves

$$2I_1 \cos 2\pi\nu\varphi_1'(hkl)/W(0)$$

and

$$2I_2 \cos 2\pi\nu\varphi_2'(hkl)/W(0).$$

To separate the waves $x(\nu)$ is multiplied by the distribution function $w'(\nu)$ which has a range narrower than $W(\varphi)$ on the φ axis {note that $w'(\nu)$ here is the modification of the Gaussian function $\exp[-\nu^2/(2\sigma^2)]$}, and then the product of $x(\nu)$ and $w'(\nu)$ is Fourier transformed. As seen in Fig. 2, the intensity pattern has been clearly separated into each peak, corresponding to its exact diffraction angle.

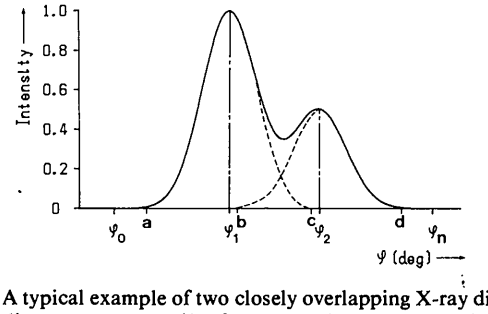

Fig. 1. A typical example of two closely overlapping X-ray diffraction lines. $a = \varphi_1 - \varphi_w/2$, $b = \varphi_2 - \varphi_w/2$, $c = \varphi_1 + \varphi_w/2$, $d = \varphi_2 + \varphi_w/2$, where φ_w is the distributed width of the function $W(\varphi)$.

3. Analytical process

Values of intensities and 2θ obtained by a diffractometer must be registered in a discrete numerical series to be processed by a computer. The number of data points N must satisfy $N = 2^m$, where m is an arbitrary positive integer. A set of intensity data for two overlapping reflections can be expressed as follows:

$$X(\varphi) = \{[I_1/W(0)]W[\varphi - \varphi_1'(hkl)] + [I_2/W(0)]W[\varphi - \varphi_2'(hkl)]\} \times \sum_{p=0}^{N-1} \delta(\varphi - \Delta\varphi p) = X(\Delta\varphi p) \quad (6)$$

where $2\theta = \varphi$. The intensity $X(p)$ at any position p is

$$X(p) = [I_1/W(0)]W(p - n_1) + [I_2/W(0)]W(p - n_2), \quad (7)$$

where $\varphi_1'(hkl) = \Delta\varphi n_1$, $\varphi_2'(hkl) = \Delta\varphi n_2$ are the theoretical diffraction angles from $K\alpha_1$ and $K\alpha_2$ radiation, respectively.

Firstly, in order to produce a wave pattern $U(k)$ on the ν axis, expressed by

$$U(k) = \sum_{p=1-N}^{N-1} X(p) \exp(2\pi i k p/2N), \quad (8)$$

the inverse fast Fourier transform (IFFT) must be adopted to the numerical series $X(p)$. The ordinary IFFT method (Papoulis, 1977) produces in the negative domain a numerical series $X(-p)$ symmetrical with regard to $p = 0$, and evaluates $U(k)$ on the ν axis by calculating $X(p)$ from $p = 1 - N$ to $p = N - 1$. This method takes a considerable time because the calculating process requires double the quantity of

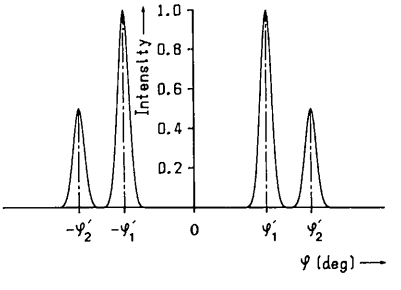

Fig. 2. An example of the X-ray diffraction pattern completely separated into two diffraction lines by the new analytical method.

data. To avoid this disadvantage, therefore, a new analytical method has been developed. The new analytical method deals with the data obtained by using the inverse fast Fourier transform that has been deduced from the inverse Fourier transform, given by

$$U(k) = 2\,\mathrm{Re}\left[\sum_{p=0}^{N-1} X(p)\exp(2\pi ikp/2N)\right]. \quad (9)$$

This equation is a modification of (8). $U(k)$, calculated from $k=0$ to $k=2N-1$ using (9), represents the product of the numerical series $x(k)$ of the wave which combines the two cosine waves with different frequencies on the ν axis, and the numerical series $w(k)$ of the distribution function, as follows:

$$\begin{aligned} U(k) &= x(k)w(k) \\ &= \{[2I_1/W(0)]\cos(2\pi n_1 k/2N) \\ &\quad + [2I_2/W(0)]\cos(2\pi n_2 k/2N)\}w(k). \end{aligned} \quad (10)$$

Next, the distribution function $w(k)$ is estimated from the envelope of $U(k)$ to give $x(k)$, which is informative of the spectral position of the X-ray diffraction. Thus

$$x(k) = U(k)/w(k).$$

$x(k)$ is then multiplied by $w'(k)$, of which the spectral distribution is narrower than $W(\varphi)$ on the φ axis. Therefore $U'(k) = x(k)w'(k)$. Here $w'(k)$ is the Gaussian function, given by

$$w'(k) = \exp[-2s^2k^2/(2N-1)^2], \quad (11)$$

its median value is 1, the parameter s determines the distribution range, and its value is a real number $6 \le s \le 8$ which is less than 2/5 of the parameter which determines the distribution range of $w(k)$ on the ν axis. [The value of the parameter of the estimated function $w(k)$ was about 20.]

Finally, the fast Fourier transform (FFT) is applied to the $U'(k)$ obtained and the discrete numerical series describing the X-ray diffraction intensity pattern calculated from $U'(k)$ is then given by

$$X'(p) = \sum_{k=0}^{2N-1} U'(k)\exp(-2\pi ipk/2N). \quad (12)$$

Therefore, the intensity distributions in the vicinity of $K\alpha_1$ and $K\alpha_2$ have clearly been separated. Determining the peaks by noise elimination and by adopting the interpolation method brings out the precise diffraction angles $2\theta_1(hkl)$ and $2\theta_2(hkl)$. A flowchart of the whole procedure is shown in Fig. 3.

4. Experimental and analytical results

A diffraction pattern was measured by an X-ray powder diffractometer using V-filtered Cr $K\alpha$ radiation at 292 (1) K. The specimen is Brazilian quartz powder (α-SiO_2), which is a commonly used standard sample for the calibration of an X-ray powder diffractometer.

The heavily overlapping diffraction intensities between $K\alpha_1$ ($\lambda_1 = 2{\cdot}28962$ Å) and $K\alpha_2$ ($\lambda_2 = 2{\cdot}29351$ Å) (*International Tables for X-ray Crystallography*, 1962) for the 110 reflection were measured in the range 54·90 to 56·18° with a step width of 0·01°; the 128 pieces of data were entered into a personal computer as a discrete numerical series. The observed diffraction pattern and the pattern separated into $K\alpha_1$ and $K\alpha_2$ in this analysis are shown in Figs. 4(*a*) and (*b*), respectively. The diffraction pattern in Fig. 4(*a*) cannot be separated into $K\alpha_1$ and $K\alpha_2$ peaks by means of graph-drawing or ordinary peak-searching methods, but the present method can distinguish the overlapping diffraction lines and gives precise diffraction angles for $K\alpha_1$ and $K\alpha_2$. The analysed values for 2θ of $K\alpha_1$ and $K\alpha_2$ were 55·55 (6) and 55·67 (5)° respectively, and they agree with the theoretical angles within an accuracy of 0·011°.

The slightly overlapping diffraction intensity of the 302 reflections was measured between $2\theta = 130{\cdot}30$ and 132·86° with a step width of 0·01°, giving 256 pieces of data. The analysed peaks of $K\alpha_1$ and $K\alpha_2$ are in good agreement with the observed peaks as found by graph drawing or by the ordinary routines of the automated diffractometer. The analysed 2θs of $K\alpha_1$ and $K\alpha_2$ were respectively 131·48 (8) and 131·93 (0)° and agree with the theoretical angles of α-SiO_2 within an accuracy of 0·007°.

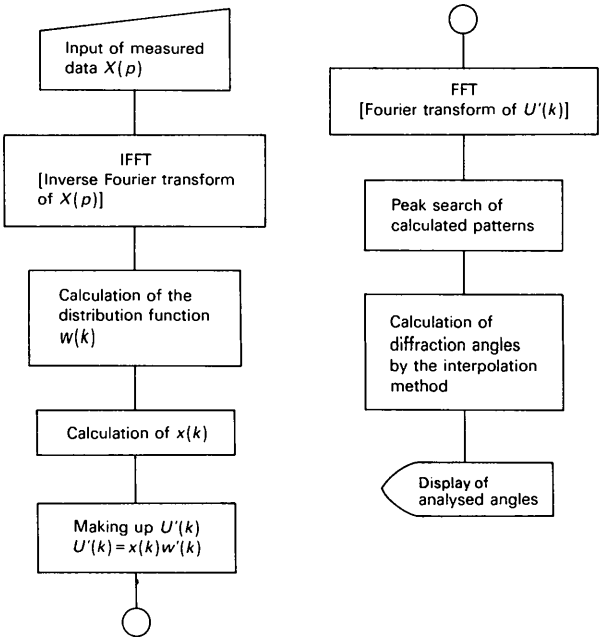

Fig. 3. Flowchart for the calculation of precise diffraction angles.

The diffraction lines from the (212), (203) and (301) planes of α-SiO_2 are known as the pentafold lines and are used to examine the resolving power of an X-ray diffractometer. In fact, the fourth line is an overlapping line consisting of $K\alpha_1$ and $K\alpha_2$ diffractions from the (301) and (203) planes respectively. Fig. 5 shows the observed and analysed results of the 512 pieces of data relating to the diffraction intensities of α-SiO_2 which appeared as the pentafold lines between $2\theta = 110{\cdot}68$ and $115{\cdot}80°$. Table 1 shows a comparison of the analysed and theoretical diffraction angles, $2\theta_a$ and $2\theta_{th}$, by Cr $K\alpha$ characteristic X-rays for α-SiO_2. The lattice constants used for the calculation of $2\theta_{th}$ were determined using all the back-reflection lines of Cr $K\alpha_1$ at 292 (1) K. These values are calculated through the use of the *Universal Crystallographic Computation Program System* program *LC*3 containing a least-squares refinement, reported by Sakurai (1967). The lattice constants obtained were in good agreement with the literature values (Helwege, 1975). As shown in Fig. 5(*b*) and Table 1, the analysed result has distinctly separated the six diffraction angles.

Table 1. *Comparison of analysed and theoretical diffraction angles*

Miller indices	Characteristic X-rays	Analysed value (°) $2\theta_a$	$\Delta 2\theta_a$ *	Theoretical value (°) $2\theta_{th}$	$\Delta 2\theta_{th}$ *
(110)	Cr $K\alpha_1$	55·55 (6)	0·11 (9)	55·56 (1)	0·10 (3)
	Cr $K\alpha_2$	55·67 (5)		55·66 (4)	
(212)	Cr $K\alpha_1$	111·87 (4)	0·29 (4)	111·88 (9)	0·28 (9)
	Cr $K\alpha_2$	112·16 (8)		112·17 (8)	
(203)	Cr $K\alpha_1$	112·76 (4)	0·29 (7)	112·77 (6)	0·29 (4)
	Cr $K\alpha_2$	113·06 (1)		113·07 (0)	
(301)	Cr $K\alpha_1$	113·14 (4)	0·28 (6)	113·15 (3)	0·29 (6)
	Cr $K\alpha_2$	113·43 (0)		113·44 (9)	
(302)	Cr $K\alpha_1$	131·48 (8)	0·44 (2)	131·48 (9)	0·43 (4)
	Cr $K\alpha_2$	131·93 (0)		131·92 (3)	

The theoretical values are determined by lattice constants of α-SiO_2, $a = 4{\cdot}9124$ and $c = 5{\cdot}4039$ Å.

* $\Delta 2\theta$ is the difference between $K\alpha_1$ and $K\alpha_2$ diffraction angles from the same diffraction plane.

5. Discussion

In analysis of X-ray powder diffraction intensity patterns, there are some unavoidable errors owing to the facts that the patterns are asymmetrical and that their peaks shift towards smaller θ, depending upon the level plane of the specimen, the vertical diversion of some incident beam, and the absorption by the specimen of some of the incident beam. The degree of the shift in θ is expressed as follows (Wilson, 1950):

$$\Delta\theta = -\frac{\sin 2\theta}{4\mu L} + \frac{t\cos\theta}{L[\exp(2\mu t/\sin\theta) - 1]} - \frac{A^2 \sin 2\theta}{6L^2}, \quad (13)$$

where μ is the linear absorption coefficient of the specimen, L is the distance between the specimen

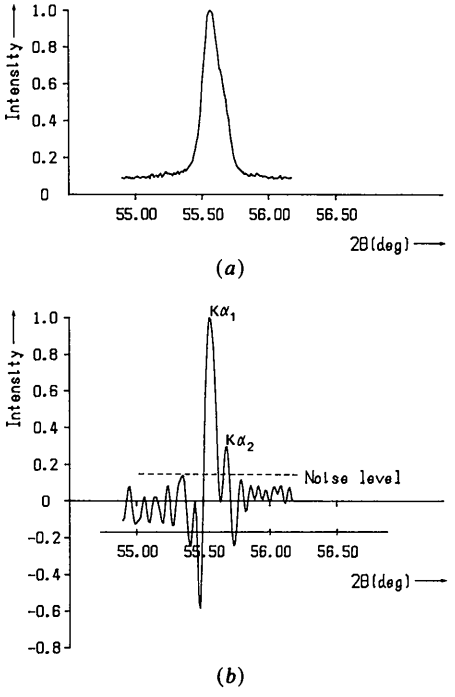

Fig. 4. (*a*) The observed heavily overlapping diffraction line from the (110) plane of α-SiO_2. (*b*) The diffraction lines from the (110) plane are separated into two lines from $K\alpha_1$ and $K\alpha_2$ radiation by the new analytical method.

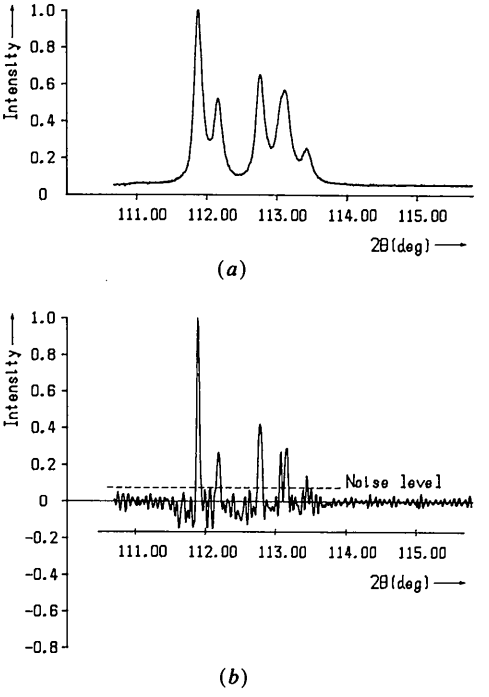

Fig. 5. (*a*) The pentafold lines of α-SiO_2 measured by the X-ray diffractometer. (*b*) The six diffraction lines of α-SiO_2 are separated into the $K\alpha_1$ and $K\alpha_2$ diffraction lines from the observed pentafold lines.

and the counter slit, t is the thickness of the specimen and $2A$ is the breadth of the spot on which the incident beam falls. In this case, where the vertical diversion of the beam is neglected, both t and A are variable factors in the experiment. If the value of $\mu = 143\ cm^{-1}$, estimated from the mass absorption coefficients of oxygen and silicon (Cullity, 1978) and the density of SiO_2, and the goniometer radius of $L = 175$ mm are entered into (13), $\Delta\theta$ is found to be less than $9 \times 10^{-3\circ}$ for $2\theta > 90°$. On the other hand, the analytical process of a personal computer is effective to six figures and its precision of calculation is better than 0·001°. The difference between $2\theta_a$ and $2\theta_{th}$ is at most 0·02° because the goniometer has a precision of $2\theta = 0{\cdot}01°$ and is scanned with a step width of 0·01° in 2θ. All errors involved in the analysis can therefore be reduced through the mechanical accuracy of the goniometer. Consequently, it is definitely possible by adopting this analytical method to obtain a higher analytical accuracy when the accuracy of the goniometer is improved and the step width is reduced.

The authors thank Dr T. Fujii of the National Research Institute for Metals for his encouragement and advice.

References

BETTS, J. A. (1970). *Signal Processing, Modulation and Noise*, p. 244. English Language Book Society.

BRACEWELL, R. N. (1978). *The Fourier Transform and its Application*, pp. 69-97. New York: McGraw-Hill.

COOLEY, J. W. & TUKEY, J. W. (1965). *Math. Comput.* **19**, 297-301.

CULLITY, B. D. (1978). *Elements of X-ray Diffraction*, 2nd ed., p. 152. Reading, MA: Addison-Wesley.

HELLWEGE, K. H. (1975). *Zahlenwerte und Funktionen aus Naturwissenschaften und Technik (Landolt-Börnstein)*, Gruppe III, Band 7, b1, p. 261. Berlin: Springer Verlag.

International Tables for X-ray Crystallography (1962). Vol. III. Birmingham: Kynoch Press. (Present distributor D. Reidel, Dordrecht.)

PAPOULIS, A. (1977). *Signal Analysis*, pp. 79-88. New York: McGraw-Hill.

PHILIPS (1983). *Scientific and Analytical Equipment Manual of Software for the Automated Powder Diffractometer System PW-1700*. Eindhoven: Philips.

SAKURAI, T. (1967). *Nippon Kessho Gakkaishi*, p. 99.

WILSON, A. J. C. (1950). *J. Sci. Instrum.* **27**, 321.

Acta Cryst. (1987). A**43**, 216-226

On the Structure and Symmetry of Incommensurate Phases. A Practical Formulation

BY J. M. PEREZ-MATO, G. MADARIAGA, F. J. ZUÑIGA AND A. GARCIA ARRIBAS

Departamento de Fisica, Facultad de Ciencias, Universidad del Pais Vasco, Apdo 644, *Bilbao, Spain*

(*Received* 17 *April* 1986; *accepted* 23 *September* 1986)

Abstract

The structural description, symmetry and diffraction properties of incommensurate modulated phases are revised using a real-space framework. The superspace formalism usually employed is reformulated using a practical description where no multidimensional geometrical constructions are needed. The incommensurate structural distortion is described in terms of 'atomic modulation functions' where the internal space is only considered as a continuous label for the cells of the non-distorted structure. Hence, no atomic positions or thermal tensors in a multidimensional space are defined. By this means and with the introduction of the concept of 'atomic modulation factors' a general expression for the structure factor is proposed which constitutes a direct generalization of the standard expression for a commensurate structure. The concept of superspace symmetry is reduced in this approach to a simple relation between the defined atomic modulation functions, which can be directly translated by means of the structure-factor expression into the symmetry and extinction rules of the diffraction diagram. The advantages of superspace formalism in the analysis of commensurate modulated phases are also discussed. The use of superspace groups for describing the symmetry of superstructures, contrary to some recent claims, does not formally reduce the number of structural parameters but may often allow some of them to be neglected.

1. Introduction

In the last few years, the structural analysis of incommensurate (IC) modulated phases has greatly progressed through the introduction of the superspace symmetry concept (de Wolff, 1974, 1977; Janner & Janssen, 1977, 1979, 1980; Yamamoto, 1982*b*). The number of IC structures which are determined using superspace formalism is increasing constantly (van Aalst, den Hollander, Peterse & de Wolff, 1976;

0108-7673/87/020216-11$01.50